CrossMark

TECHNICAL ARTICLE

X-ray powder diffraction reference patterns for $Bi_{1-x}Pb_xOCuSe$

W. Wong-Ng,[1,a] Y. Yan,[2] J.A. Kaduk,[3] and X.F. Tang[2]
[1]*Materials Measurement Science Division, National Institute of Standards and Technology, Gaithersburg, Maryland 20899*
[2]*State Key Laboratory of Advanced Technology for Materials Synthesis and Processing, Wuhan University of Technology, Wuhan, Hubei 430070, China*
[3]*Department of Chemistry, Illinois Institute of Technology, Chicago, Illinois 60616*

(Received 9 April 2016; accepted 21 May 2016)

The structures and powder X-ray reference diffraction patterns of the "natural superlattice" series $Bi_{1-x}Pb_xOCuSe$ ($x = 0$, 0.02, 0.04, 0.06, 0.08, and 0.10) have been investigated. As the ionic radius of Pb^{2+} is greater than that of Bi^{3+}, the unit-cell volume of $Bi_{1-x}Pb_xOCuSe$ increases progressively from $x = 0$ to 0.1, namely, from 137.868(5) to 139.172(11) Å^3, as expected. The structure of $Bi_{1-x}Pb_xOCuSe$ is built from $[Bi_{2(1-x)}Pb_{2x}O_2]^{2(1-x)+}$ layers normal to the *c*-axis alternating with $[Cu_2Se_2]^{2(1-x)-}$ fluorite-like layers. Pb substitution in the Bi site of $Bi_{1-x}Pb_xOCuSe$ leads to the weakening of the "bonding" between the $[Bi_{2(1-x)}Pb_{2x}O_2]^{2(1-x)+}$ and the $[Cu_2Se_2]^{2(1-x)-}$ layers. Powder patterns of $Bi_{1-x}Pb_xOCuSe$ were submitted to be included in the Powder Diffraction File.
© *2016 International Centre for Diffraction Data*. [doi:10.1017/S0885715616000361]

Key words: thermoelectric material, $Bi_{1-x}Pb_xOCuSe$, powder X-ray reference patterns, crystal structure

I. INTRODUCTION

The demand for new thermoelectric materials for energy conversion applications has been growing over recent years. Compounds with low-dimensional layered structures have attracted increasing interest in thermoelectric research because of their high-power factor, *P*, where $P = S^2\sigma$ (S = Seebeck coefficient and σ = electrical conductivity). The efficiency of thermoelectric energy conversion is related to the dimensionless figure of merit (*ZT*) of a thermoelectric material, given by $ZT = S^2\sigma T/k$, where *T* is the absolute temperature, and *k* is thermal conductivity (Tritt and Subramanian, 2006). The search for high-efficiency materials (high *ZT*) for waste heat conversion and refrigeration applications continues to be a high-priority activity in the energy R&D community.

To improve thermoelectric properties, various strategies have been pursued, including lowering of thermal conductivity. "Natural superlattice" materials, in which layers with excellent electronic transport properties are combined with a second type of layer, which serves as a phonon scatterer, in general exhibit low thermal conductivities (Luu and Vaquelro, 2013). "Natural superlattice" oxides that have been studied extensively include $NaCo_2O_4$ (Terasaki *et al*., 1997), $Ca_3Co_4O_9$ (Masset *et al*., 2000; Mikami *et al*., 2002; Grebille *et al*., 2004; Wong-Ng *et al*., 2007, 2010; Otani *et al*., 2007), and $Bi_2Sr_2Co_2O_x$ (Wang *et al*., 2009).

Quaternary oxychalcogenides *MBOCh* [*M* = lanthanide (La) and Bi; *B* = Cu and Ag; *Ch* = S, Se, and Te (Palazzi, 1981; Kusainova *et al*., 1994; Zhu *et al*., 1994; Popovkin *et al*., 1998; Charkin *et al*., 1999; Takase *et al*., 2007; Hiramatsu *et al*., 2008; Richard *et al*., 2012)] are known to adopt the layered type crystal structure of the LaOCuS and LaOAgS types (Palazzi *et al*., 1980; Palazzi, 1981; Palazzi and Jaulmes, 1981), and can also be considered as "natural superlattice" materials. The interest in the Bi analogs of the LaCuO*Ch* system is partly because of the electronic configuration of Bi (Richard *et al*., 2012). On the basis of the electronic structures obtained by photoelectron spectroscopy and density functional theory calculations, the BiCuO*Ch* phases have been found by Hiramatsu *et al*. (2008) to have small band gaps, because of the contribution of the Bi 6*p* orbitals to the conduction band minima. Richard *et al*. (2012) obtained the band gap value of BiCuOSe single crystals (0.82 eV) from infrared transmission measurements. Many of the La oxychalcogenides are, however, wide band gap (≥3 eV) transparent semiconductors (Ueda *et al*., 2000, 2003; Ueda and Hosono, 2002), which possess interesting optical properties (Hiramatsu *et al*., 2008).

According to Luu and Vaqueiro (2013), the effect of increasing dopant of Pb^{2+} on the Bi site of the Pb-doped $Bi_{1-x}Pb_xOCuSe$ series is the reduction of the band gap size, leading to a systematic decrease of electrical resistivity. For this family of oxychalcogenides, *p*-type conduction is often observed, and is attributed to the formation of a covalent hybridized band between Cu and Se atoms at the top of the valence band. Another source of the *p*-type behavior could be related to copper deficiency, which can generate mobile holes. Figure 1 shows the *ZT* as a function of *x* in $Bi_{1-x}Pb_xOCuSe$. It is observed that *ZT* at 673 K is enhanced by ≈50% (Luu and Vaqueiro, 2013).

There are two goals for this study. First, $Bi_{1-x}Pb_xOCuSe$ ($x = 0$, 0.02, 0.04, 0.06, 0.08, and 0.1) compounds are investigated for the effect of Pb substitution in the Bi site on the resulting structure. Since X-ray diffraction (XRD) is a non-destructive technique for phase identification, XRD patterns are especially important for phase characterization; therefore, the second goal of this investigation was to determine the

[a]Author to whom correspondence should be addressed. Electronic mail: winnie.wong-ng@nist.gov

https://doi.org/10.1017/S0885715616000361 Published online by Cambridge University Press

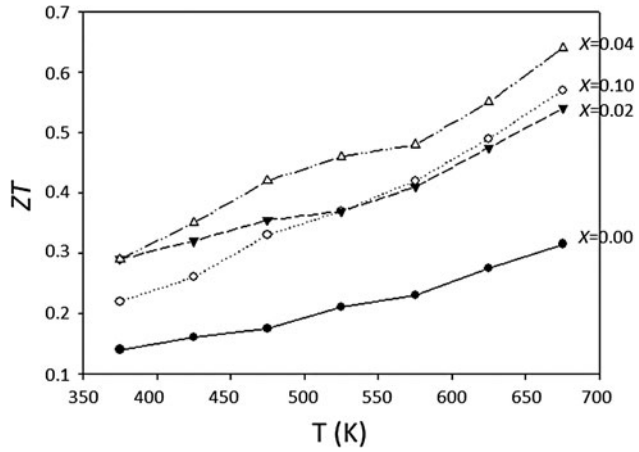


Figure 1. Figure of merit, ZT of $Bi_{1-x}Pb_xOCuSe$ as a function of temperature (Luu and Vaquelro, 2013).

experimental patterns for $Bi_{1-x}Pb_xOCuSe$ ($x = 0$, 0.02, 0.04, 0.06, 0.08, and 0.1), and to make them widely available through submission to the Powder Diffraction File (PDF) (2016). The pattern of BiOCuSe has been reported in PDF 46–296 by Antipov and D'yachenko (1993).

II. EXPERIMENTAL

A. Sample preparation

Samples were prepared by the self-propagating high-temperature synthesis (SHS) technique (Su *et al.*, 2014). High-purity powders of elemental Bi, Cu, and Se were blended in a mortar and pestle, and pelletized under ≈100 MPa. The pellets were ignited using an electric heater, and the product was obtained in under 1 min. The powder was obtained by grinding the reacted pellets.

B. X-ray Rietveld refinements and powder reference patterns

(The purpose of identifying the equipment in this paper is to specify the experimental procedure. Such identification does not imply recommendation or endorsement by the National Institute of Standards and Technology.)

The $Bi_{1-x}Pb_xOCuSe$ ($x = 0$, 0.02, 0.04, 0.06, 0.08, and 0.10) compounds were mounted on a zero-background cell. The X-ray powder patterns were measured on a Bruker D2 Phaser diffractometer (30 kV, 10 mA, 5°–130° 2θ in 0.020 2144° steps, 0.5 s $step^{-1}$) equipped with a LynxEye position-sensitive detector. For all samples, the lower window of the detector electronics was increased from its default value of 0.11–0.19 V to minimize the effects of fluorescence.

The Rietveld refinement technique (Rietveld, 1969) with software suite GSAS (Larson and von Dreele, 2004) was used to determine the structure of $Bi_{1-x}Pb_xOCuSe$. The structure of BiOCuSe (Richard *et al.*, 2012) reported previously was used as the starting model for the refinements. The site occupancies of Bi/Pb as prepared were used in $Bi_{1-x}Pb_xOCuSe$. The pseudo-Voigt function (profile function #2) was used for the refinements (Howard, 1982; Thompson *et al.*, 1987). Background function #1 (shifted Chebyshev function with six terms) in combination with the CW X-ray profile (functions #2) were used for the refinements. Profile coefficients LX, ptec, and shft were refined. Peak tails are ignored where the intensity is below 0.005 times the peak.

Reference patterns were obtained with a Rietveld pattern decomposition technique. Using this technique, the reported peak positions were derived from the extracted integrated intensities, and positions calculated from the lattice parameters. When peaks are not resolved at the resolution function, the intensities are summed, and an intensity-weighted d-spacing is reported.

III. RESULTS AND DISCUSSION

Table I provides the crystallographic data for $Bi_{1-x}Pb_xOCuSe$ ($x = 0$, 0.02, 0.04, 0.06, 0.08, and 0.1) which include cell parameters, Z values, and calculated density, and refinement results, respectively. Table II gives the pertinent atomic coordinates and displacement parameters. Table III summarizes the bond distances and angles. The $Bi_{1-x}Pb_xOCuSe$ compounds are tetragonal with space group $P4/nmm$ (129), $Z = 2$. Our data agreed with that given by Luu and Vaqueiro (2013).

Figure 2 shows the XRD pattern of the $Bi_{1-x}Pb_xOCuSe$ ($x = 0.6$) powder and the results of the Rietveld analysis. The observed (crosses), calculated (solid line), and difference XRD patterns (bottom), are shown. The difference pattern is plotted at the same scale as the other patterns up to 60°2θ. At higher angles, the scale has been magnified five times. The results indicate that the sample is a single phase.

As the ionic radius of Pb^{2+} (1.29 Å) is greater than that of Bi^{3+} (1.17 Å) (Shannon, 1976), a monotonically increasing trend of unit-cell volume as a function of x of $Bi_{1-x}Pb_xOCuSe$ is evidenced in Figure 3 [from 137.868(3) to 139.772(11) $Å^3$ for $x = 0$ to 0.1, respectively]. This increase is more noticeable along the c-axis (Table I).

TABLE I. Crystal data for $Bi_{1-x}Pb_xOCuSe$ ($x = 0$, 0.02, 0.04, 0.06, 0.08, and 0.1).

	$x = 0$	0.02	0.04	0.06	0.08	0.10
Molecular weight	367.48	367.45	367.41	367.38	367.34	367.31
Cell constants						
a (Å)	3.929 43(5)	3.930 77(6)	3.932 71(6)	3.933 42(7)	3.934 62(7)	3.934 95(13)
c (Å)	8.909 23(15)	8.9411(2)	8.952 00(15)	8.9646(2)	8.9769(2)	8.9882(3)
V ($Å^3$)	137.868(5)	138.148(5)	138.454(2)	138.699(6)	138.973(6)	139.172(11)
D_c (g cm^{-3})	8.852	8.833	8.813	8.797	8.778	8.765
R	0.0364	0.0396	0.0388	0.0427	0.0417	0.0538
R_{WP}	0.0470	0.0517	0.0499	0.0571	0.0577	0.0766
$R_{Expected}$	0.0460	0.0430	0.0435	0.0435	0.0491	0.0450

Crystal system tetragonal $P4/nmm$ (no. 129), $Z = 2$, $T = 298$ K, radiation Cu$K\alpha$. Values inside the brackets represent standard deviations (SD).

https://doi.org/10.1017/S0885715616000361 Published online by Cambridge University Press

TABLE II. Positional (*x, y, z*) and displacement parameters for $Bi_{1-x}Pb_xOCuSe$ ($x = 0$, 0.02, 0.04, 0.06, 0.08, and 0.1).

Atom		x	y	z	Site Occ.	U_{iso}	Wyckoff symbol
(i) $x = 0$							
	Bi1	0.25	0.25	0.140 62(12)	1.0	0.0179(3)	2c
	Cu3	0.75	0.25	0.5	1.0	0.0231(11)	2b
	Se4	0.25	0.25	0.6749(2)	1.0	0.0175(8)	2c
	O5	0.75	0.25	0.0	1.0	0.026(5)	2a
(ii) $x = 0.02$							
	Bi1/Pb2	0.25	0.25	0.139 90(12)	0.98/0.02	0.0296(4)	2c
	Cu3	0.75	0.25	0.5	1.0	0.0404(14)	2b
	Se4	0.25	0.25	0.6741(3)	1.0	0.0303(10)	2c
	O5	0.75	0.25	0.0	1.0	0.024(5)	2a
(iii) $x = 0.04$							
	Bi1	0.25	0.25	0.140 04(12)	0.96/0.04	0.0296(4)	2c
	Cu3	0.75	0.25	0.5	1.0	0.0391(13)	2b
	Se4	0.25	0.25	0.6737(3)	1.0	0.0333(10)	2c
	O5	0.75	0.25	0.0	1.0	0.030(5)	2a
(iv) $x = 0.06$							
	Bi1	0.25	0.25	0.139 28(14)	0.94/0.06	0.0313(4)	2c
	Cu3	0.75	0.25	0.5	1.0	0.0360(15)	2b
	Se4	0.25	0.25	0.6728(3)	1.0	0.0324(11)	2c
	O5	0.75	0.25	0.0	1.0	0.022(5)	2a
(v) $x = 0.08$							
	Bi1	0.25	0.25	0.138 82(14)	0.92/0.08	0.0230(4)	2c
	Cu3	0.75	0.25	0.5	1.0	0.0301(15)	2b
	Se4	0.25	0.25	0.6723(3)	1.0	0.0237(11)	2c
	O5	0.75	0.25	0.0	1.0	0.014(5)	2a
(vi) $x = 0.10$							
	Bi1	0.25	0.25	0.1376(2)	0.9/0.1	0.0297(7)	2c
	Cu3	0.75	0.25	0.5	1.0	0.032(2)	2b
	Se4	0.25	0.25	0.6713(4)	1.0	0.026(2)	2c
	O5	0.75	0.25	0.0	1.0	0.013(7)	2a

Crystal system tetragonal *P4/nmm* (no. 129), $Z = 2$, $T = 298$ K, radiation Cu$K\alpha$. The values inside the brackets refer to SD.

Figure 4 gives the crystal structure of $Bi_{1-x}Pb_xOCuSe$ along the [010] direction. The structure of $Bi_{1-x}Pb_xOCuSe$ is built from $[Bi_{2(1-x)}Pb_{2x}O_2]^{2(1-x)+}$ layers normal to the *c*-axis alternating with $[Cu_2Se_2]^{2(1-x)-}$ fluorite-like layers. The $[(Bi/Pb)_2O_2]$ layers are built of slightly distorted $(Bi/Pb)_4O$ tetrahedra that share (Bi/Pb)–(Bi/Pb) edges. The two different (Bi/Pb)–O–(Bi/Pb) bond angles (three of each type) are shown in Table III. The effect of Pb doping on the Bi site of the BiOCu*Ch* structure is the increasing separation of the $[Bi_{2(1-x)}Pb_{2x}O_2]^{2(1-x)+}$ and the $[Cu_2Se_2]^{2(1-x)-}$ layers, therefore weakening the bonding between them, as evidenced from the progressively increasing of the *c*-parameter. Therefore the electrical resistivity and Seebeck coefficient of $Bi_{1-x}Pb_xOCuSe$ decrease systematically with increasing Pb^{2+} levels (Luu and Vaqueiro, 2013).

The Cu^{1+} cation site has a D_{2d} symmetry, with Cu coordinated by Se^{2-} anions forming distorted $CuSe_4$ tetrahedra. The two tetrahedral angles α and β are shown in Figure 5. Comparing to an ideal tetrahedron, the tetrahedra are compressed in the *ab*-plane and elongated along the *c*-axis (increase of the β angle and decrease of the α angle). In the $[Cu_2Se_2]$ layers, the distorted $CuSe_4$ tetrahedra share Se–Se edges forming $[Cu_2Se_2]$ layers. The Se–Cu–Se angles are given in Table III. With increasing Pb content, there is a reduction of the distortion of the $CuSe_4$ tetrahedra.

The coordination of (Bi/Pb) is a distorted square antiprism with four O in one base and four Se in the other, typical of Sillen phases (Dolgikh and Kholodkovskaya, 1992) (Figure 6). The (Bi/Pb)–O distances ranging from 2.3316(6) to 2.3237(9) Å in $Bi_{1-x}Pb_xOCuSe$ (from $x = 0$ to 0.1, respectively). These bond distances are not significantly different from the Bi–O distance found in Bi_2O_2Se (2.32 Å) (Boller, 1973).

TABLE III. Selected bond distances and angles for $Bi_{1-x}Pb_xOCuSe$ ($x = 0$, 0.02, 0.04, 0.06, 0.08, and 0.10).

	$x = 0$	0.02	0.04	0.06	0.08	0.1
Distances (Å)						
Bi/Pb–O ×4	2.3316(6)	2.3296(6)	2.3320(6)	2.3296(7)	2.3288(7)	2.3237(9)
Bi/Pb–Se ×4	3.2300(13)	3.2392(14)	3.2425(14)	3.252(2)	3.258(2)	3.270(2)
Cu–Se ×4	2.5099(14)	2.5070(15)	2.5068(15)	2.503(2)	2.502(2)	2.498(2)
Angles (°)						
O–Bi/Pb–O ×2	114.84(4)	115.05(5)	114.96(4)	115.18(5)	115.30(15)	115.71(7)
O–Bi/Pb–O ×4	106.86(2)	106.75(2)	106.80(2)	106.69(2)	106.64(2)	106.45(3)
Se–Cu–Se ×3 (α)	112.78(4)	112.67(5)	112.62(5)	112.50(5)	112.46(5)	112.32(7)
Se–Cu–Se ×3 (β)	103.03(8)	103.25(9)	103.33(9)	103.56(10)	103.65(10)	103.92(13)

The values inside the brackets refer to SD.

https://doi.org/10.1017/S0885715616000361 Published online by Cambridge University Press

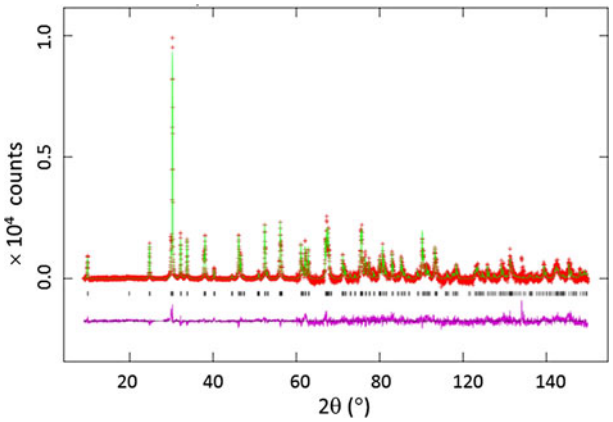


Figure 2. (Colour online) Rietveld pattern for $Bi_{1-x}Pb_xOCuSe$ ($x = 0.06$). The observed (crosses), calculated (solid line), and difference XRD patterns (bottom), are shown. The difference pattern is plotted at the same scale as the other patterns up to 60°2θ. At higher angles, the scale has been magnified five times.

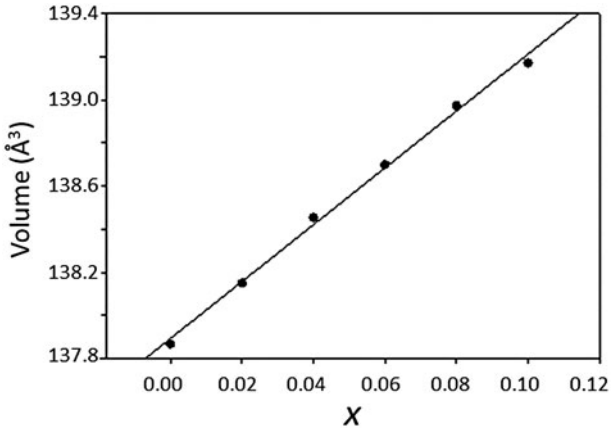


Figure 3. Plot of unit-cell volume, V, of $Bi_{1-x}Pb_xOCuSe$ as a function of x. A monotonic trend of increase of V as a function of x is observed.

An example of the reference patterns, $Bi_{1-x}Pb_xOCuSe$ ($x = 0.6$), is given in Table IV. In this pattern, the strongest peak in the pattern is assigned an intensity of 999 and other lines are scaled relative to this value. The d-spacing values are calculated values from refined lattice parameters. The intensity values reported are integrated intensities (rather than peak heights) calculated from corresponding profile parameters. For peaks containing more than one reflection that can still be resolved, intensity-weighted calculated d-spacing, along with the observed integrated intensity and the hkl indices of both peaks (for "M"), or the hkl indices of the strongest peak (for "+") are used. For peaks that are not resolved within the instrumental resolution, the intensity-weighted average d-spacing and the summed integrated intensity value are used. In the case of a cluster, unconstrained profile fits often reveal the presence of multiple peaks, even when they are closer than the instrumental resolution. In this situation, both d-spacing and intensity values are reported independently. All patterns have been submitted for inclusion in the Powder Diffraction File (PDF).

IV. SUMMARY

The crystal structure of the $Bi_{1-x}Pb_xOCuSe$ series of compounds ($x = 0$, 0.02, 0.04, 0.06, 0.08, and 0.1) have been determined. The effect of Pb substitution in the Bi site has been found to lengthen the c-axis, causing a greater separation of the $[Bi_{2(1-x)}Pb_{2x}O_2]^{2(1-x)+}$ and the $[Cu_2Se_2]^{2(1-x)-}$

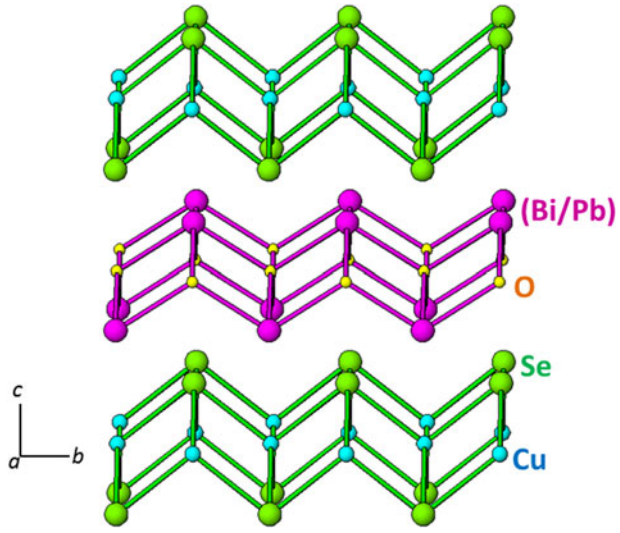


Figure 4. (Colour online) View of the crystal structure of $Bi_{1-x}Pb_xOCuSe$ along the [010] direction. The structure of $Bi_{1-x}Pb_xOCuSe$ consists of alternating $[Bi_{2(1-x)}Pb_{2x}O_2]^{2(1-x)+}$ and $[Cu_2Se_2]^{2(1-x)-}$ layers.

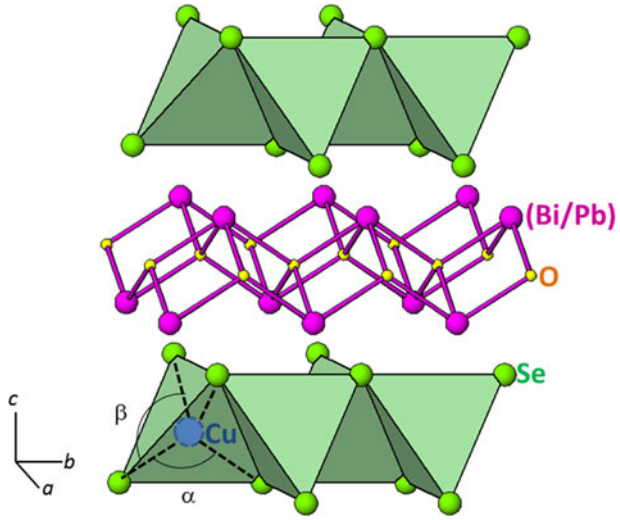


Figure 5. (Colour online) The $CuSe_4$ polyhedra in $Bi_{1-x}Pb_xOCuSe$ are shown. Selected bond angles α and β in $Bi_{1-x}Pb_xOCuSe$ are indicated.

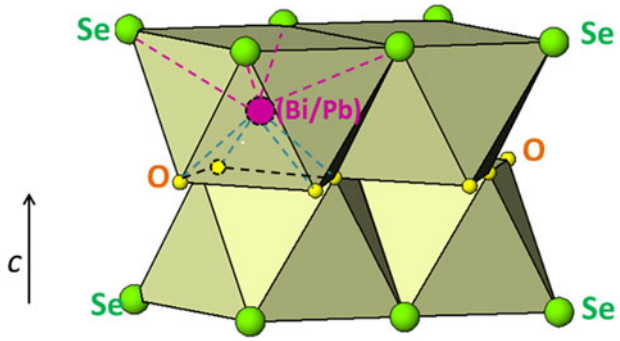


Figure 6. (Colour online) A distorted square antiprism around the central (Bi/Pb) in $Bi_{1-x}Pb_xOCuSe$ is shown.

https://doi.org/10.1017/S0885715616000361 Published online by Cambridge University Press

TABLE IV. X-ray powder pattern for $Bi_{1-x}Pb_xOCuSe$ ($x = 0.06$).

d_{cal}	I_{obs}	h	k	l	d_{cal}	I_{obs}	h	k	l
8.9646	75	0	0	1	4.4823	20	0	0	2
3.6020	128	1	0	1	2.9882	108	0	0	3
2.9565	999	1	0	2	2.7814	204	1	1	0
2.6564	168	1	1	1	2.3794	95	1	0	3
2.3633	184	1	1	2	2.2412	39	0	0	4
2.0359	7	1	1	3	1.9667	237	2	0	0
1.9472	91	1	0	4	1.9210	9	2	0	1
1.7929	42	0	0	5	1.7451	270	1	1	4
1.7262	46	2	1	1	1.6428	50	2	0	3
1.6373	294	2	1	2	1.6314	38	1	0	5
1.5159	40	2	1	3	1.5070	10	1	1	5
1.4941	32	0	0	6	1.4782	28	2	0	4
1.3967	33	1	0	6	1.3907	68	2	2	0
1.3837	44	2	1	4	1.3250	25	2	0	5
1.3162	12	1	1	6	1.2608	16	2	2	3
1.2584	53	3	0	2	1.2557	28	2	1	5
1.2439	33	3	1	0	1.2320	25	3	1	1
1.2177	11	1	0	7	1.2007	8	3	0	3
1.1986	28	3	1	2	1.1897	39	2	0	6
1.1817	18	2	2	4	1.1633	38	1	1	7
1.1483	5	3	1	3	1.1388	28	2	1	6
1.1317	9	3	0	4	1.0989	7	2	2	5
1.0876	67	3	1	4	1.0830	8	3	2	1
1.0777	18	1	0	8	1.0732	11	2	0	7
1.0600	52	3	2	2	1.0583	6	3	0	5
1.0354	4	2	1	7	1.0248	3	3	2	3
1.0220	3	3	1	5	1.0180	14	2	2	6
0.9855	4	3	0	6	0.9834	9	4	0	0
0.9809	10	3	2	4	0.9736	6	2	0	8
0.9656	22	1	0	9	0.9559	4	3	1	6
0.9486	4	4	1	1	0.9451	21	2	1	8
0.9421	9	2	2	7	0.9378	4	1	1	9
0.9341	5	4	0	3	0.9331	40	4	1	2
0.9320	11	3	2	5	0.9271	6	3	3	0
0.9222	4	3	3	1	0.9162	9	3	0	7
0.9088	3	4	1	3	0.9005	4	4	0	4
0.8923	31	3	1	7	0.8811	16	3	2	6
0.8795	34	4	2	0	0.8778	12	4	1	4
0.8726	9	2	2	8	0.8668	44	2	1	9
0.8622	4	4	0	5	0.8567	11	3	3	4
0.8532	6	1	1	10					

Crystal system tetragonal $P4/nmm$ (no. 129), $Z = 2$, $T = 298$ K, radiation Cu$K\alpha$. $a = 3.933\,42(7)$, $c = 8.9646(2)$, and $V = 138.699(6)$ Å^3. The particular peak that has the strongest intensity in the entire pattern is assigned an intensity of 999 and other lines are scaled relative to this value. The d-spacing values are calculated values from refined lattice parameters, and "I" represents integrated intensity values.

layers, and the $CuSe_4$ tetrahedra to be elongated along the c-axis, therefore systematically decreasing the electrical resistivity and Seebeck coefficient. Powder XRD patterns for these compounds have been submitted for inclusion in the PDF.

ACKNOWLEDGEMENTS

Partial financial support from ICDD is acknowledged.

Antipov, E. and D'yachenko, O. (**1993**) PDF 00-045-296, International Centre for Diffraction Data, 12 Campus Blvd., Newtown Squares, PA 19073-3273, USA.

Boller, H. (**1973**). "Die Kristallstruktur von Bi_2O_2Se," Monatsh, Chem. **104**, 916.

Charkin, D. O., Akopyan, A. V., and Dolgikh, V. A. (**1999**). "New oxochalcogenides of rare-earth elements with the stucture of LaOAgS," Russ. J. Inorg. Chem. **44**, 833.

Dolgikh, V. A. and Kholodkovskaya, L. N. (**1992**). "Crystal chemistry of layered metal oxyhalides and oxychalcogenides (sillen phases)," Zh. Neorg. Khim. **37**(5), 970–985.

Grebille, D., Lambert, S., Bourée, F., and Petricek, V. (**2004**). "Contribution of powder diffraction for structure refinements of aperiodic misfit cobalt oxides," J. Appl. Crystallogr. **37**, 823–831.

Hiramatsu, H., Yanagi, H., Kamiya, T., Ueda, K., Hirano, M., and Hosono, H. (**2008**). "Crystal structure, optoelectronic properties, and electronic structures of layered oxychalcogenides MCuOCh (M = Bi, La; Ch = S, Se, Te): effects of electronic configurations of M^{3+} ions," Chem. Mater. **20**, 326–334.

Howard, C. J. (**1982**). "The approximation of asymmetric neutron powder diffraction peaks by sums of Gaussians," J. Appl. Crystallogr. **15**(6), 615–620.

Kusainova, A. M., Berdonosov, P. S., Akselrud, L. G., Kholodkovskaya, L. N., Dolgikh, V. A., and Popovkin, B. A. (**1994**). "New layered compounds with the general composition (MO)(CuSe), where M = Bi, Nd, Gd, Dy, and BiOCuS: synthesis and crystal structure," J. Solid State Chem. **112**, 189–191.

Larson, A. C. and von Dreele, R. B. (**2004**). *General Structure Analysis System (GSAS)* (Los Alamos National Laboratory Report LAUR 86-748). Los Alamos, USA.

Luu, S. D. N. and Vaquelro, P. (**2013**). "Synthesis, structural characterization and thermoelectric properties of $Bi_{1-x}Pb_xOCuSe$," J. Mater. Chem A **1**, 12270–12275.

Masset, A. C., Michel, C., Maignan, A., Hervieu, M., Toulemonde, O., Studer, F., and Raveau, B. (**2000**). "Misfit-layered cobaltite with an anisotropic giant magnetoresistance: $Ca_3Co_4O_9$," Phys. Rev. B **62**, 166–175.

Mikami, H., Itaka, K., Kawaji, H., Wang, Q. J., Koinuma, H., and Lippmaa, M. (**2002**). "Rapid synthesis and characterization of $(Ca_{1-x}Ba_x)_3Co_4O_9$ thin films using combinatorial methods," Appl. Surf. Sci. **197**, 442–447.

Otani, M., Lowhorn, N. D., Schenck, P. K., Wong-Ng, W., and Green, M. (**2007**). "A high-throughput thermoelectric screening tool for rapid construction of thermoelectric phase diagrams," Appl. Phys. Lett. **91**, 132102.

Palazzi, M. (**1981**). "Préparation el affinement de la structure de (LaO)CuS," Acad. Sci., Paris, C.R. Ser. II **292**, 789.

Palazzi, M. and Jaulmes, J. (**1981**). "Structure du Conducteur Ionique (LaO) AgS," Acta Crystallogr. B **37**, 1337.

Palazzi, M., Carcaly, C., and Flahaut, J. (**1980**). "Un nouveau conducteur ionique (LaO)AgS Original Research Article," J. Solid State Chem. **35**, 150.

PDF, Powder Diffraction File (**2015**). Produced by International Centre for Diffraction Data, 12 Campus Blvd., Newtown Squares, PA 19073-3273, USA.

Popovkin, B. A., Kusainova, A. M., Dolgikh, V. A., and Aksel'rud, L. G. (**1998**). "New layered phases of the MOCuX (M = Ln, Bi; X = S, Se, Te) family: a geometric approach to the explanation of phase stability," Russ. J. Inorg. Chem. **43**, 1471.

Richard, A. P., Russell, J. A., Zaktuayev, A., Zakharov, L. N., Keszler, D. A., and Tate, J. (**2012**). "Synthesis, structure, and optical proeprties of BiCuOCh (Ch=S, Se, and Te)," J. Solid State Chem. **187**, 15–19.

Rietveld, H. M. (**1969**). "A profile refinement method for nuclear and magnetic structures," J. Appl. Crystallogr. **2**, 65–71.

Shannon, R. D. (**1976**). "Revised effective ionic radii and systematic studies of interatomie distances in halides and chalcogenides," Acta Crystallogr. A **32**, 751–767.

Su, X., Fu, F., Yan, Y., Zheng, G., Liang, Q., Cheng, X., Yang, D., Chi, H., Tang, X., Zhang, Q., and Uher, C. (**2014**). "Self-propagating high-temperature synthesis for compound thermoelectrics and new criterion for combustion processing," Nat. Commun. **5**, 4908.

Takase, K., Sato, K., Shoji, O., Takahashi, Y., Takano, Y., Sekizawa, K., Kuroiwa, Y., and Goto, M. (**2007**). "Charge density distribution of transparent p-type semiconductor (LaO)CuS," Appl. Phys. Lett. **90**, 161916.

Terasaki, I., Sasago, Y., and Uchinokura, K. (**1997**). "Large thermoelectric power in $NaCo_2O_4$ single crystals", Phys. Rev. B **56**, 12685–12687.

Thompson, P., Cox, D. E., and Hastings, J. B. (**1987**). "Rietveld refinement of Debye–Scherrer synchrotron X-ray data from Al_2O_3", J. Appl. Crystallogr. **20**, 79–83.

Tritt, T. M. and Subramanian, M. A. (guest editors) (**2006**). *Harvesting Energy through Thermoelectrics: Power Generation and Cooling* (MRS Bulletin, Materials Research Soc.), Materials Research Society, 506 Keystone Dr, Warrendale, PA 15086, pp. 188–195.

https://doi.org/10.1017/S0885715616000361 Published online by Cambridge University Press

Ueda, K. and Hosono, H. (**2002**). "Band gap engineering, band edge emission, and p-type conductivity in wide-gap $LaCuOS_{1-x}Se_x$ oxychalcogenides," J. Appl. Phys. **91**, 4768.

Ueda, K., Inoue, S., Hirose, S., Kawazoe, H., and Hosono, H. (**2000**). "Transparent *p*-type semiconductor: LaCuOS layered oxysulfide," Appl. Phys. Lett. **77**, 2701.

Ueda, K., Takafuji, K., Hiramatsu, H., Ohta, Kamiya, T., Hirano, M., and Hosono, H. (**2003**). "Electrical and optical properties and electronic structures of LnCuOS (Ln = La–Nd)," Chem. Mater., **15**, 3692.

Wang, S., Venimadhav, A., Guo, S., Chen, K., Li, Q., Soukiassian, A., Schlom, D. G., Pan, X. Q., Wong-Ng, W., Vaudin, M. D., Cahill, D. G., and Xi, X. X. (**2009**). "Structural and thermoelectric properties of $Bi_2Sr_2Co_2O_y$ thin films on $LaAlO_3$ (100) and fused silica substrates," Appl. Phys. Lett. **94**, 022110.

Wong-Ng, W., Hu, Y. F., Vaudin, M. D., He, B., Otani, M., Lowhorn, N. D., and Li, Q. (**2007**). "Texture analysis of a $Ca_3Co_4O_9$ thermoelectric film on Si (100) substrate," J. Appl. Phys. **102**(3), 33520.

Wong-Ng, W., Liu, G., Martin, J., Thomas, E., Lowhorn, N., and Otani, M. (**2010**). "Phase compatibility of the thermoelectric compounds in the Sr–Ca–Co–O system," J. Appl. Phys. **107**, 033508.

Zhu, W. J., Huang, Y. Z., Dong, C., and Zhao, Z. X. (**1994**). "Synthesis and crystal structure of new rare-earth copper oxyselenides: *R*CuSeO (*R*=La, Sm, Gd and Y)," Mater. Res. Bull. **29**, 143.

https://doi.org/10.1017/S0885715616000361 Published online by Cambridge University Press